Supplementary information

Mireia Sainz-Menchón,[a] Iñigo González de Arrieta,[*a] Telmo Echániz,[b] Karam Nader,[c]

Maite Insausti,[c,d] Aurélien Canizarès [e], Olivier Rozenbaum,[e] and Gabriel A. López[a]

[a] *Physics Department, University of the Basque Country (UPV/EHU), E-48940 Leioa, Spain.*

[b] *Applied Mathematics, University of the Basque Country (UPV/EHU), E-48013 Bilbao, Spain.*

[c] *Departamento Química Orgánica e Inorgánica, Facultad de Ciencia y Tecnología, University of the Basque Country (UPV/EHU), Sarriena s/n, 48940 Leioa, Spain.*

[d] *BCMaterials, Basque Center for Materials, Applications and Nanostructures, UPV/EHU Science Park, 48940 Leioa, Spain.*

[e] *Université d'Orléans, CNRS, CEMHTI UPR 3079, Orléans, France*

inigo.gonzalezdearrieta@ehu.eus

1 Raman vibrational modes:

According to group theory, the Raman spectrum of the magnetite spinel structure exhibits five Raman active modes (A_{1g} + $3T_{2g}$ + E_g) [1], the indexation of which has caused some controversy in the literature during the past two decades. During these years a large number of experimental studies, as well as some computational ones, were conducted in order to reach an accurate indexation [2-5], but one of the most accepted interpretations nowadays is that presented by Shebanova *et al.* based on polarized Raman studies [6,7]. The reported wavenumber values for these vibrational modes are $\nu_{T2g(1)}$=193 cm^{-1}, ν_{Eg}=306 cm^{-1}, $\nu_{T2g(2)}$=450-490 cm^{-1}, $\nu_{T2g(3)}$= 538 cm^{-1} and ν_{A1g}= 668 cm^{-1}. Nevertheless, the typical room temperature Raman spectrum of magnetite nanoparticles is characterized by a high-intensity band corresponding to A_{1g} found at ≈660-670 cm^{-1}, together with two low-intensity bands corresponding to E_g and $T_{2g(3)}$ located around ≈300 and ≈530 cm^{-1}, respectively. The observation of the bands corresponding to $T_{2g(1)}$ and $T_{2g(2)}$ is not always reported.

In the case of γ-Fe_2O_3, even if group theory predicts the same number of Raman active vibrational modes as for Fe_3O_4, a spectrum consisting of three vibrational bands is typically recorded. In this case, the main A_{1g} is located around ≈ 710 cm^{-1}, blue-shifted compared to that of magnetite. Two lower intensity broad bands corresponding to the vibrational modes T_{2g} and E_g are usually located at ≈ 350 cm^{-1} and ≈500 cm^{-1}, respectively[2, 4].

+

2 Supplementary tables:

Table S1: Computed cell parameter applying the DICVOL04 cell refinement method. It must be taken into account that, given a cubic cell structure, *a=b=c* and $\alpha = \beta = \gamma = 90°$. The lattice parameter values (*a)* for magnetite and maghemite have been taken from references [8-10]

Material	***a* (Å)**
Fe_3O_4[8,9]	8.396
γ -Fe_2O_3[10]	8.33
40:120_S	8.363 ± 0.005
40:120_L	8.352 ± 0.004
40:115_S	8.346 ± 0.005
40:125_S	8.342 ± 0.005
40:115_S_OAm	8.331 ± 0.008

Table S2: position and mixing parameter (η) of the fitted Raman peaks.

	λ=633 nm				**λ=514 nm**			
	A_{1g} Fe_3O_4		A_{1g} γ-Fe_2O_3		A_{1g} Fe_3O_4		A_{1g} γ-Fe_2O_3	
	Position	η	Position	η	Position	η	Position	η
40:120_S	670	0.998	702	0.988	664	0.999	706	0.986
40:120_L	670	0.999	707	0.999	666	0.999	714	0.981
40:115_S	670	0.970	704	0.862	664	0.999	704	0.999
40:125_S	670	0.996	710	0.999	662	0.971	714	0.999
40:115_S_OAm	670	0.999	716	0.999	665	0.999	706	0.997

Table S3: Raman and infrared active modes corresponding to each space groups related to γ -Fe_2O_3. Built using the Bilbao Crystallographic Server [1]

Space group	Wyckoff positions	IR active modes	Raman active modes
Fd-3m	8a	-	T_{2g}
	16d	$2T_{1u}$	-
	32e	$2T_{1u}$	$A_{1g} + E_g + T_{2g}$
$P4_132$, $P4_332$	4b	$1T_1$	$E + T_2$
	8c	$3T_1$	$A_1 + 2E + 3T_2$
	12d	$5T_1$	$A_1 + 3E + 4T_2$
	24e	$9T_1$	$3A_1 + 6E + 9T_2$
$P4_12_12$, $P4_32_12$	4a	$A_2 + 2E$	$A_1 + 2B_1 + B_2 + 3E$
	8b	$3A_2 + 6E$	$3A_1 + 3B_1 + 3B_2 + 6E$

3 Supplementary figures:

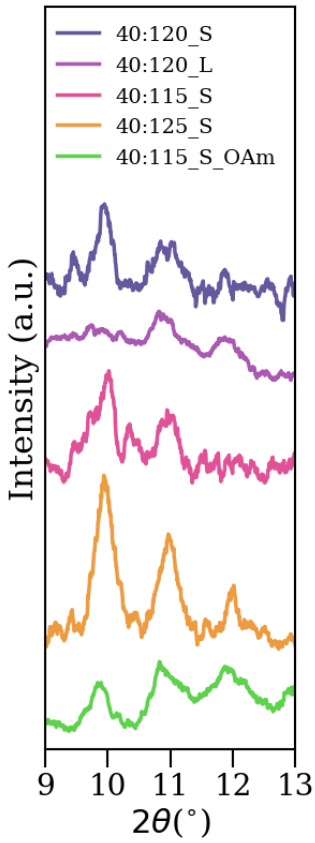

Figure S1: a vertically enlarged section of the diffractogram to enhance the visualization of peaks (210) and (211).

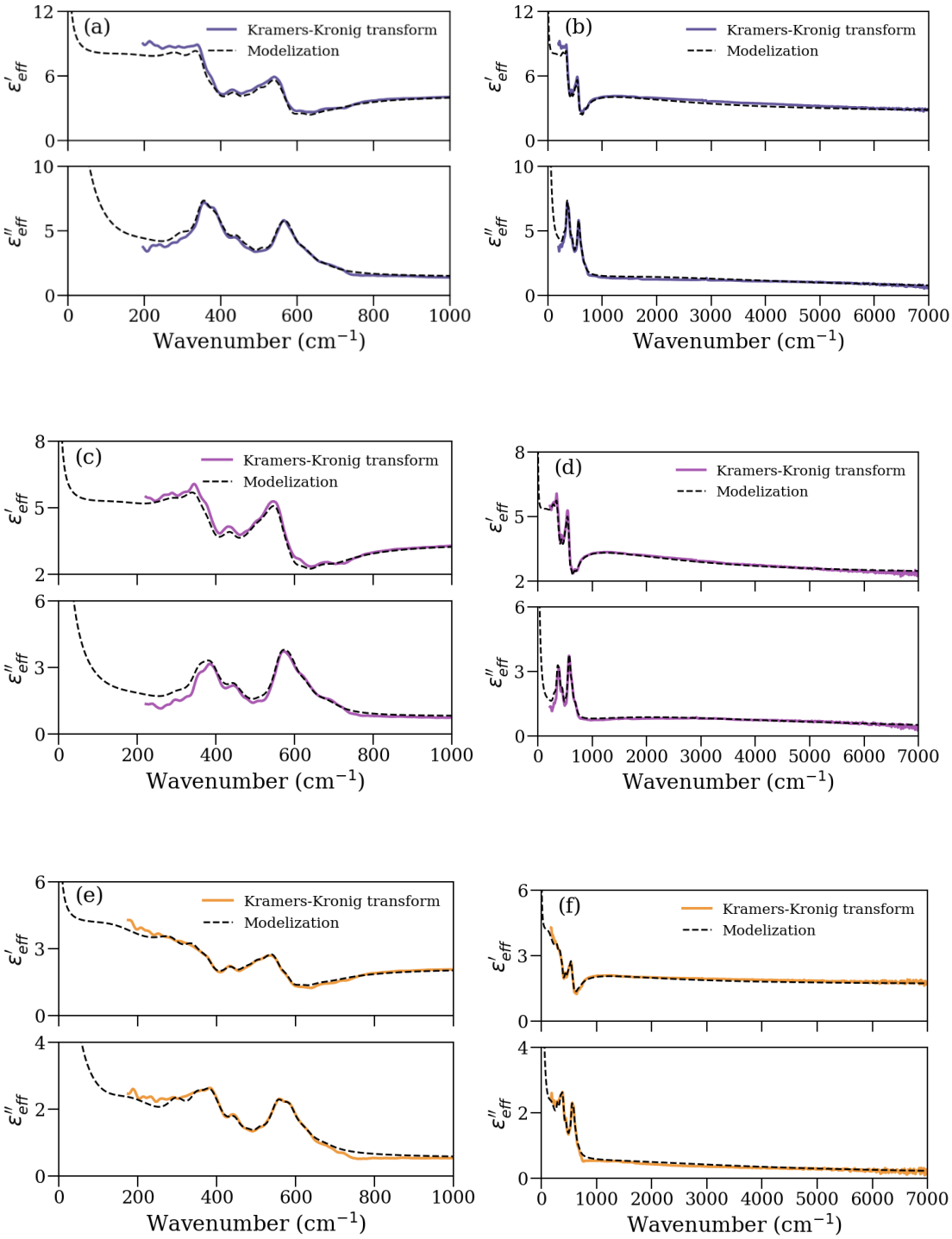

Figure S2: The real and imaginary parts of the effective permittivity of the samples computed using Kramers-Kronig analysis (solid lines) and obtained from the modelization (dashed lines) for samples 40:120_S (FIR (a), MIR (b)), 40:120_L (FIR (c), MIR (d)) and 40:125_S (FIR (e), MIR (f)).

4 References

[1] M.I. Aroyo, J. M. Perez-Mato, D. Orobengoa, E. Tasci, G. de la Flor and A. Kirov. *Bulgarian Chemical Communications*, 2011, 43,183-197

[2] I. Chamritski and G. Burns, *The Journal of Physical Chemistry B*, 2005, 109, 4965–4968.

[3] L. Gasparov, D. Tanner, D. Romero, H. Berger, G. Margaritondo and L. Forro, *Physical Review B*, 2000, 62, 7939.

[4] D. L. De Faria, S. Venâncio Silva and M. T. de Oliveira, *Journal of Raman Spectroscopy*, 1997, 28, 873–878.

[5] S.P. Schwaminger, D. Bauer, P. Fraga- García, F.E. Wagner and S. Berensmeier. *CrystEngComm*, 2017, 19, 246-255

[6] O. N. Shebanova and P. Lazor. *Journal of Raman Spectroscopy*, 2003, 34, 845-852.

[7] M. Testa-Anta, M.A. Ramos-Docampo, M. Comesaña-Hermo, B. Rivas-Murias and V. Salgueiriño. *Nanoscale Advances*. 2019, 1, 2086-2103

[8] O. Lemine, K. Omri, B. Zhang, L. El Mir, M. Sajieddine, A. Alyamani and M. Bououdina, *Superlattices and Microstructures*, 2012, 52, 793–799.

[9] S. Nasrazadani and A. Raman, *Corrosion Science*, 1993, 34, 1355–1365.

[10] C. Pecharromán, T. Gonzalez-Carreno and J. E. Iglesias, *Physics and Chemistry of Minerals*, 1995, 22, 21–29.